ЖЭТФ, 2011, том 140, вып. 3 (9), стр. 527–535 

# ANDREEV SPECTROSCOPY OF FeSe: EVIDENCE FOR TWO-GAP SUPERCONDUCTIVITY

***Ya. G. Ponomarev*** [a], ***S. A. Kuzmichev*** [a], ***M. G. Mikheev*** [a], ***M. V. Sudakova*** [a], ***S. N. Tchesnokov*** [a], ***T. E. Shanygina*** [a], ***O. S. Volkova*** [a], ***A. N. Vasiliev*** [a]*, ***Th. Wolf*** [b]

[a] *Low Temperature Physics and Superconductivity Department, Moscow State University 119991, Moscow, Russia*

[b] *Karlsruher Institut für Technologie, Institut für Festkörperphysik D-76021, Karlsruhe, Germany*

Received December 21, 2010

Current–voltage characteristics (CVCs) of Andreev superconductor–constriction–superconductor (ScS) contacts in polycrystalline samples of FeSe with the critical temperature $T_C = (12 \pm 1)$ K have been measured using the break-junction technique. In Sharvin-type nanocontacts, two sets of subharmonic gap structures were detected due to multiple Andreev reflections, indicating the existence of two nodeless superconducting gaps $\Delta_L = (2.75 \pm 0.3)$ meV and $\Delta_S = (0.8 \pm 0.2)$ meV. Well-shaped CVCs for stacks of Andreev contacts with up to five contacts were observed due to the layered structure of FeSe (the intrinsic multiple Andreev reflections effect). An additional fine structure in the CVCs of Andreev ScS nanocontacts is attributed to the existence of a Leggett mode. A linear relation between the superconducting gap $\Delta_L$ and the magnetic resonance energy $E_{magres} \approx 2\Delta_L$ is found to be valid for layered iron pnictides.

Among a wide range of iron-based superconductors [1, 2], the binary compound FeSe has the simplest crystal structure and a moderate critical temperature $T_C$ = (8–13) K [3, 4]. The transition temperature $T_C$ can be increased to 37 K by applying external pressure [5, 6] or totally suppressed by tensile strain [7]. It is generally accepted that superconductivity exists only in tetragonal phase [3, 8, 9]. At ambient-pressure FeSe is not magnetically ordered, but its magnetic properties become more complicated as the external pressure increases or Se is substituted by Te [10, 11].

A layered structure is a common feature of iron-based superconductors [12]. In the case of FeSe, the Fermi surface consists of two intersecting cylindrical electron Fermi surfaces at the Brillouin zone corner and two concentric hole cylinders at the zone center, similar to FeAs-based multiband superconductors [13]. It can be expected that FeSe also belongs to the class of multiband superconductors, which have been studied intensively since the original theoretical papers [14, 15].

Initially, a two-gap model was proposed by Kresin and Wolf for cuprate superconductors [16, 17]. Experimental evidence for a two-band superconductivity in $YBa_2Cu_3O_{7-\delta}$ came from surface impedance measurements [18] and tunneling spectroscopy [19, 20]. Studies of multigap superconductivity intensified after the discovery of superconductivity in $MgB_2$ (2001) [21] and later in iron pnictides (2008) [22] (see [2, 23] for the details). The model of nodeless multigap superconductivity in FeSe was supported by experimental studies of the magnetic penetration depth [24] and quasiparticle heat transport [25].

A unique property of two-band superconductors is the existence of a collective excitation (Leggett mode) [26], which was recently detected in $MgB_2$ [27–30]. Prerequisites of the observation of the Leggett mode in iron oxypnictides were discussed in [31].

Naturally, the layered structure of iron-based superconductors triggered a search for the intrinsic Josephson effect (IJE) [32–34], and some experimental evidence for its existence in oxypnictides was recently presented [35].

Andreev spectroscopy is a powerful instrument to measure the superconducting energy gap(s) in a wide temperature range up to $T_C$ [36, 37]. A number of such

*E-mail: vasil@mig.phys.msu.ru

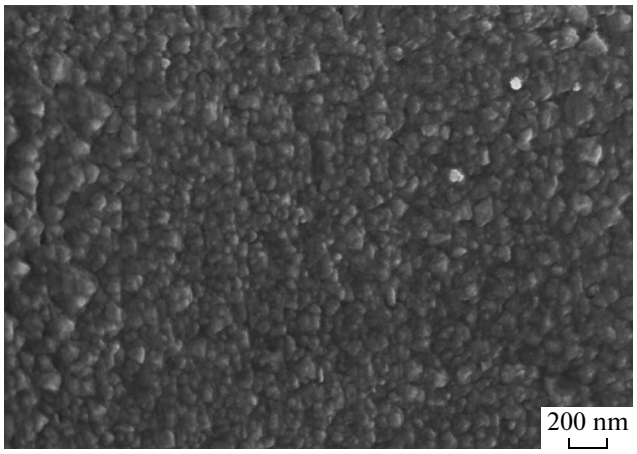


**Fig. 1.** The morphology of the sample surface as seen by electron microscopy

measurements have been performed on oxypnictides $RFeAsO_{1-x}F_x$ [38–41]. Studies of the subharmonic gap structure (SGS) in current–voltage characteristics of individual Sharvin-type ScS nanocontacts [27, 28, 41] help to gain valuable information even in the case of inhomogeneous samples. To make the SGS observable, the size $a$ of an Andreev contact should be chosen significantly smaller than the mean free path $l$ of quasiparticles (the ballistic regime) [42]. A typical size $a$ of a ballistic contact is of the order of (10–20) nm or less [38, 41], and is usually much smaller than the crystallite size in a polycrystalline sample.

Here, we present a systematic study of current–voltage characteristics of FeSe break junctions at temperatures 4.2 K $\leq T < T_C$. Polycrystalline samples of FeSe have been grown from melt by spontaneous nucleation. Powders of iron (puriss.) and selenium (99.95 %) were mixed at the molar ratio 1:1, sealed into a quartz tube and heated to 1100 °C at the rate 100 °C/h. After a holding time of 1 hour, the ampoule was cooled to 986 °C at the rate 1.3 °C/h and then quenched by taking out of the furnace. The morphology of the sample surface is illustrated by Fig. 1, where grains of typical dimensions 100 nm are clearly seen.

The quality of the samples was characterized by measurements of the temperature and field dependences of magnetization performed in the "Quantum Design" Magnetic Property Measurement System. The temperature dependence of magnetization measured in the magnetic field $B = 0.01$ T, as shown in Fig. 2, demonstrates an almost complete Meissner effect with the superconducting transition temperature $T_C$ about 10.5 K. The superconducting transition width indi-

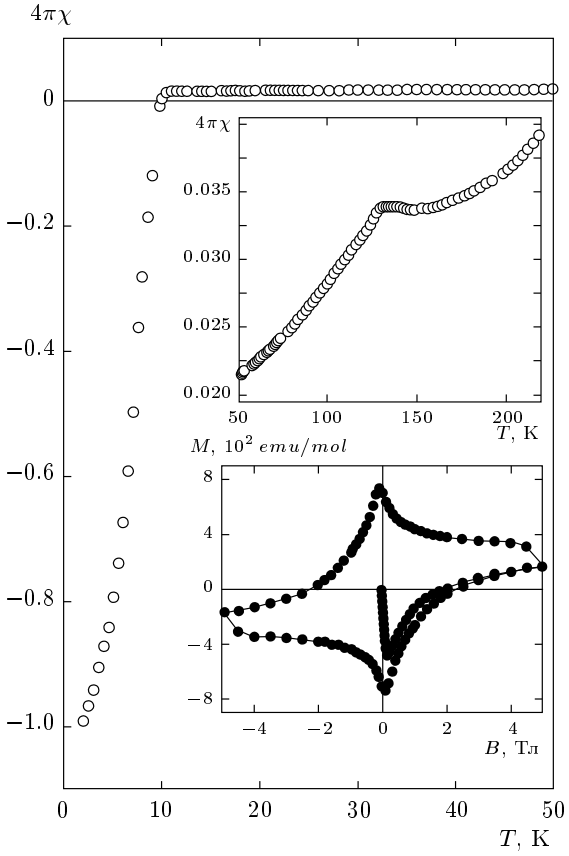


**Fig. 2.** The temperature dependence of the magnetic susceptibility $\chi$ of FeSe. The upper inset is a magnification of $\chi(T)$ in the vicinity of the magnetic due to the presumed $Fe_7Se_8$ impurity. The lower inset shows a magnetization loop in FeSe at 2 K

cates a nonuniformity of the superconducting state in the sample. At $T > T_C$, the magnetic susceptibility is positive and shows a pronounced kink at about 133 K, as can be seen in the upper inset to Fig. 2. Tentatively, this kink can be ascribed to a spin-reorientation phase transition in the impurity phase $Fe_7Se_8$. This phase is ferrimagnetic with the Curie temperature about 450 K [43]. The presence of a ferrimagnetic component in magnetization is clearly seen from finite slopes of $M$–$B$ curves, shown in the lower inset to Fig. 2. Without the correction for the demagnetizing factor, the first critical field of FeSe can be estimated as $B_{C1} = 0.225 \pm 0.025$ T at 2 K. Both the upper critical field $B_{C2}$ and the irreversibility field $B_{irr}$ were not reached in present measurements.

To produce point contacts in thin plates with dimensions about $(0.1 \times 1.0 \times 3.0)$ mm$^3$, we used the break-junction technique [41, 44]. Two current and two potential leads were attached to each plate by an In–Ga

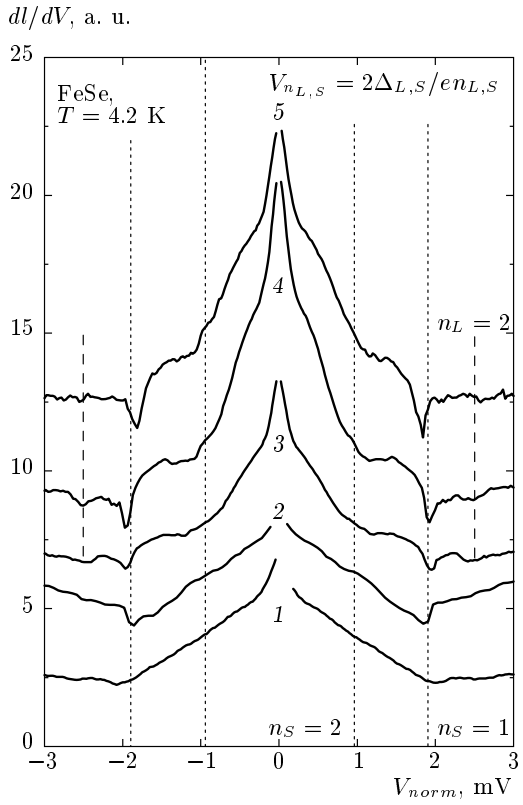


**Fig. 3.** The normalized $dI/dV$ characteristics of adjustable Andreev ScS break junctions in polycrystalline FeSe samples at $T = 4.2$ K: *1* — a single-contact FS1D02, *2* — a two-contact array FS1D01, *3*, *4* — three-contact arrays FS1D09 and FS1D10 respectively, *5* — a six-contact array FS1D13. Two sets of subharmonic gap singularities at bias voltages $V_{nL} = 2\Delta_L/en_L$ and $V_{nS} = 2\Delta_S/en_S$ are detectable ($\Delta_L = 2.5$ meV and $\Delta_S = 0.95$ meV). The dashed and dotted lines display the expected bias voltages $V_{nL}$ and $V_{nS}$

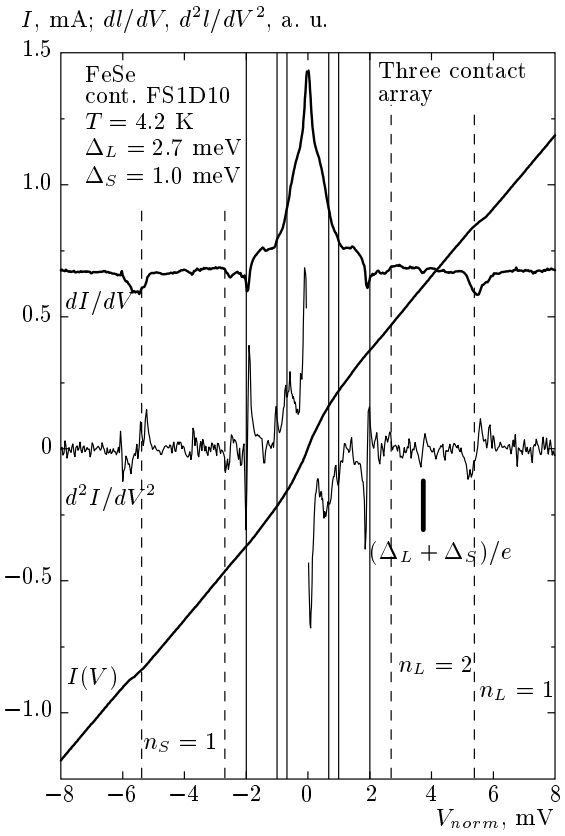


**Fig. 4.** The normalized $I(V)$, $dI/dV$, and $d^2I/dV^2$ characteristics of the Andreev ScS break junction in a polycrystalline FeSe sample (a three-contact array FS1D10) at $T = 4.2$ K. Two sets of subharmonic gap singularities at the bias voltages $V_{nL} = 2\Delta_L/en_L$ and $V_{nS} = 2\Delta_S/en_S$ are detectable ($\Delta_L = 2.7$ meV and $\Delta_S = 1.0$ meV). The dashed and solid lines respectively show the expected bias voltages $V_{nL}$ and $V_{nS}$. The vertical bar displays the expected bias voltage $(\Delta_L + \Delta_S)/e$

alloy. A crack in the sample was generated at helium temperature. The $I(V)$ and $dI(V)/dV$ characteristics of a mechanical point contact between two cryogenically cleaved surfaces were registered by a computer-controlled experimental set-up [41]. The $dI/dV$- and $d^2I/dV^2$-characteristics were measured using a standard modulation technique. A low-level AC modulation voltage (820 Hz) on potential leads of a contact was stabilized using a lock-in nanovoltmeter and computer-controlled digital AC bridge with a PID feedback signal. The differential conductance of a contact is proportional to the amplitude of the AC feedback current through the contact.

To evaluate the superconducting gap, two related methods were used: Andreev spectroscopy of individual ScS Sharvin-type contacts (the gap was calculated from SGS in $dI(V)/dV$ characteristics [45–47]) and intrinsic Andreev spectroscopy (natural stacks of Andreev contacts in the $c$-direction, the intrinsic multiple Andreev reflections effect [48, 49]). It is possible to switch between these two different regimes of measurements in one experiment simply by readjusting the contact with a micrometric screw. An additional advantage of this technique is the existence of clean cryogenically cleaved surfaces used for the contact formation.

In studying intrinsic multiple Andreev reflections effect in FeSe samples, we used natural nanosteps-and-terraces structures, which were always present on the top of atomically flat crystal surfaces [50]. The $I(V)$ characteristics of such nanosteps ($j \parallel c$) are

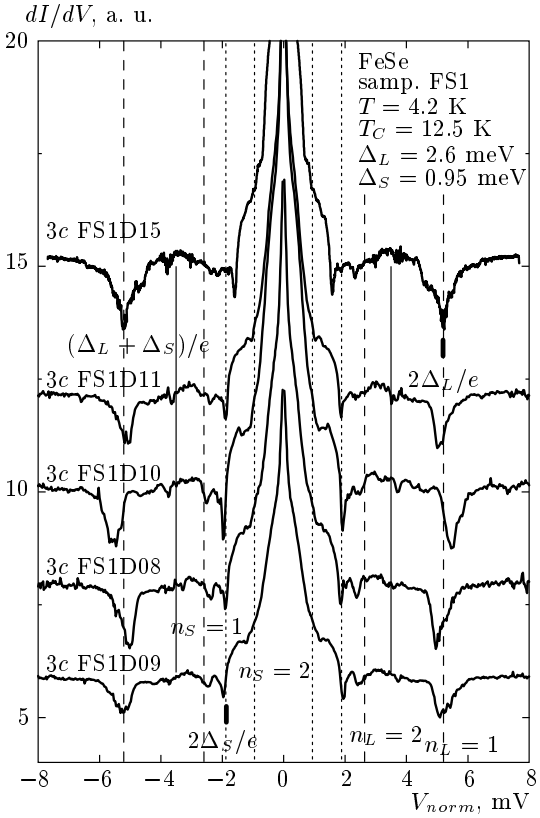


**Fig. 5.** The normalized $dI/dV$ characteristics of the Andreev ScS break junctions in a polycrystalline FeSe sample (three-contact arrays, $T_C = 12.5$ K) at $T = 4.2$ K. Two sets of subharmonic gap singularities at the bias voltages $V_{nL} = 2\Delta_L/en_L$ and $V_{nS} = 2\Delta_S/en_S$ are detectable ($\Delta_L = 2.6$ meV and $\Delta_S = 0.95$ meV). The dashed and dotted lines respectively show the expected bias voltages $V_{nL}$ and $V_{nS}$. The solid lines display the expected bias voltages $\pm(\Delta_L + \Delta_S)/e$

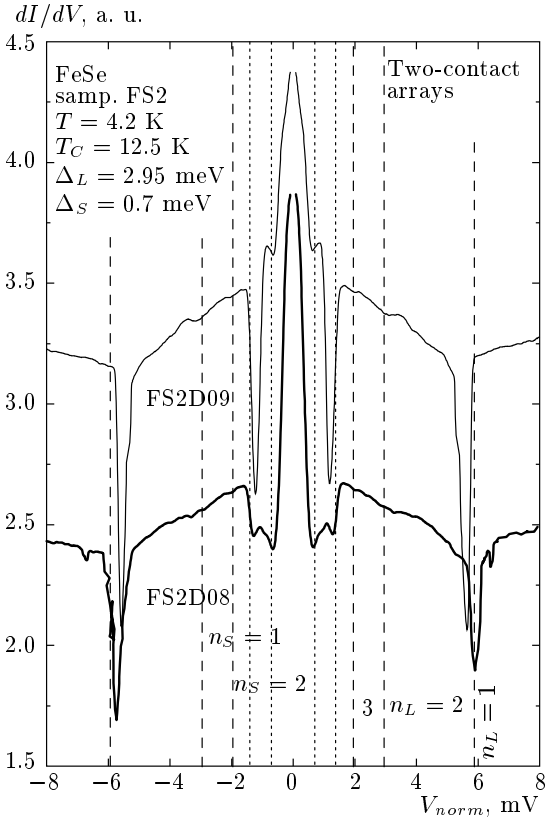


**Fig. 6.** The normalized $dI/dV$ characteristics of the Andreev ScS break junctions in a polycrystalline FeSe sample (two-contact arrays FS2D08 and FS2D09, $T_C = 12.5$ K) at $T = 4.2$ K. Two sets of subharmonic gap singularities at the bias voltages $V_{nL} = 2\Delta_L/en_L$ and $V_{nS} = 2\Delta_S/en_S$ are detectable ($\Delta_L = 2.95$ meV and $\Delta_S = 0.7$ meV). The dashed and dotted lines respectively show the expected bias voltages $V_{nL}$ and $V_{nS}$

actually characteristics of stacks of superconductor–insulator–superconductor (SIS) (or superconductor–normal metal–superconductor (SNS)) contacts due to the layered structure of the compound. In one measuring cycle, it is always possible to find several nanosteps with different heights by readjusting the contact [48, 49]. We note that nanosteps are located in between of the two surfaces forming a crack, which protects these nanosteps from being overheated by the measuring current.

The main features of $I(V)$ characteristics of ScS Sharvin-type contacts in a classical single-gap superconductor comprise a pronounced excess current at low bias voltages and a subharmonic gap structure, showing sharp dips of the differential conductance $dI/dV$ at bias voltages [45–47]:

$$V = \frac{2\Delta}{en}, \quad n = 1, 2, \ldots \tag{1}$$

Usually, SGS is explained by multiple Andreev reflections at interfaces of the point contact. In the case of a two-gap superconductor, there exist two independent SGSs, corresponding to the gaps $\Delta_L$ and $\Delta_S$. When the amplitudes of the gaps differ significantly ($\Delta_L \gg \Delta_S$) and only the channels $L \to L$ and $S \to S$ are dominant, there is no difficulty in measuring both SGSs. This type of structure was earlier observed in excess-current characteristics of ScS break junctions in $MgB_2$ [27, 28] and $LaFeAsO_{1-x}F_x$ [41]. When the $L \to S$ channel becomes significant, an additional structure appears, being most noticeable at the bias voltage $V = (\Delta_L + \Delta_S)/e$ [51]. In this investigation, we assume that the theoretical model of

Kümmel et al. [45] is applicable to our break junctions with excess-current characteristics.

The quality of the SGS strongly depends on the ratio of the mean free path $l$ to the radius of the contact area $a$ [45]. In this investigation, it was possible to observe several (up to 4) singularities in SGS and to calculate both gaps $\Delta_L$ and $\Delta_S$ with sufficient accuracy. We note that the accuracy significantly decreases when the two SGSs corresponding to two different gaps overlap. Luckily, for FeSe nanocontacts (ScS, Sharvin-type), the subharmonic gap structures are separated due to a pronounced difference in $\Delta_L$ and $\Delta_S$ values (Figs. 3–6).

Another difficulty in analyzing experimental data arise from the appearance of stacks of Andreev contacts while using the break-junction technique (due to the presence of natural nanosteps-and-terraces structures on the cleavage surfaces [50]). The bias voltage $V_{n,m} = m(2\Delta/en)$ corresponding to the subharmonic gap structure for stacks is "quantized" ($m$ is the number of contacts in a stack). We see this when we readjust the contact with a micrometric screw and the number of contacts $m$ changes. In one experiment, it is easy to obtain several contacts with different $m$. Usually, $m$ varies in the range from one to five or six. There are two important properties of current-voltage characteristics of these stacks: 1) when normalized to a single contact, the SGSs for individual contacts and stacks coincide within experimental errors (Fig. 3) and 2) the SGS in $dI/dV$ characteristics of stacks is much sharper than the SGS for individual contacts (Figs. 3–6).

There are definitely two superconducting gaps ($\Delta_L = (2.75 \pm 0.3)$ meV and $\Delta_S = (0.8 \pm 0.2)$ meV) in FeSe (Figs. 4–7, Table). The superconducting parameters in Ref. [24] (a two-band model version) are also added to Table for comparison. In accordance with the two-band model, the intraband coupling in one of the bands is weak and superconductivity in this band is induced by the "driving" band through the interband coupling (this is illustrated by model calculations shown in Fig. 2 in Ref. [52]). As a result, the zero-temperature gap ratio $2\Delta_S/k_BT_C$ for the "weak" band is significantly smaller than the BCS value (Table). This is also the case for $LaFeAsO_{1-x}F_x$ [41] and $MgB_2$ [27–29].

Additional Andreev singularities in Figs. 4 and 5 at bias voltages $V = \pm(\Delta_L + \Delta_S)/e$ are most probably caused by the opening of the $L \to S$ channel due to a strong interband scattering [51].

We estimate the local critical temperature $T_C$ of FeSe nanocontacts $T_C = (12.5 \pm 0.5)$ K from the temperature dependence of the large gap $\Delta_L(T)$ (Figs. 8 and 9). This temperature corresponds to the onset temperature of the resistive transition of a sample, measured before creation of a crack (Fig. 9). A quick decrease of the small gap $\Delta_S(T)$ (Figs. 8 and 9) qualitatively agrees with calculations in Ref. [52]. Due to a weak interband coupling ($\lambda_{ij} \ll \lambda_{ii}$), the function $\Delta_S(T)$ deviates significantly from the standard BCS dependence, but the critical temperature $T_C$ is the same for both gaps (see insets to Fig. 2 in Ref. [52]). It is worth noting that a close doublet structure of Andreev singularities for $n_S = 1$ (see Figs. 8 for example) could result from the four-band nature of the electron spectrum of FeSe [1, 2].

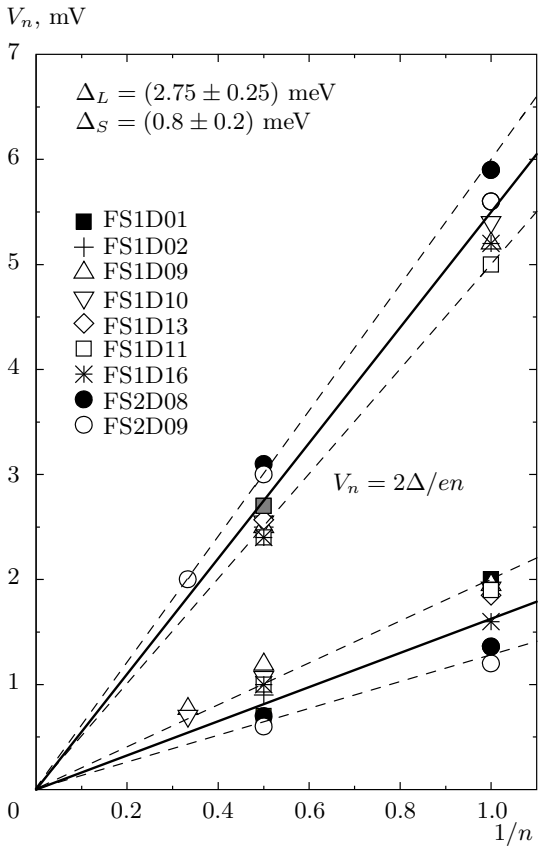


**Fig. 7.** The dependences of bias voltages $V_{nL} = 2\Delta_L/en_L$ and $V_{nS} = 2\Delta_S/en_S$ on $1/n_{L,S}$ for the investigated Andreev ScS contacts. The solid lines correspond to $\Delta_L = (2.75 \pm 0.25)$ meV and $\Delta_S = (0.8 \pm 0.2)$ meV. Dashed lines indicate spreading of data

The sharp line shape of Andreev singularities composing the SGS for a high-quality nanocontact (Fig. 6) points to nodeless gaps $\Delta_L$ and $\Delta_S$ in FeSe. This conclusion is also supported by the comparison of our experimental data (Fig. 4, the $d^2I/dV^2$ characteristic)

**Table.** Superconducting parameters of FeSe samples at $T = 4.2$ K and ambient pressure

| Sample | $T_C$, K | $\Delta_L(4.2\ \mathrm{K})$ | $\Delta_S(4.2\ \mathrm{K})$ | $2\Delta_L(0)/kT_C$ | $2\Delta_S(0)/kT_C$ |
|---|---|---|---|---|---|
| Present investigation | | | | | |
| FS1D08 (three contact array) | $12.5 \pm 1.0$ | $2.5 \pm 0.2$ | $1.0 \pm 0.2$ | $4.6 \pm 0.8$ | $1.9 \pm 0.4$ |
| FS1D09 (three contact array) | $12.5 \pm 1.0$ | $2.5 \pm 0.2$ | $1.0 \pm 0.2$ | $4.6 \pm 0.8$ | $1.9 \pm 0.4$ |
| FS2D01 (three contact array) | $12.5 \pm 1.0$ | $2.3 \pm 0.3$ | $1.1 \pm 0.2$ | $4.3 \pm 0.8$ | $2.0 \pm 0.5$ |
| FS2D09FIN (two contact array) | $12.5 \pm 1.0$ | $2.9 \pm 0.2$ | $0.6 \pm 0.1$ | $5.4 \pm 0.8$ | $1.1 \pm 0.3$ |
| Data from [24] | | | | | |
| FeSe | 8.3 | 1.63 | 0.38 | 4.59 | 1.07 |

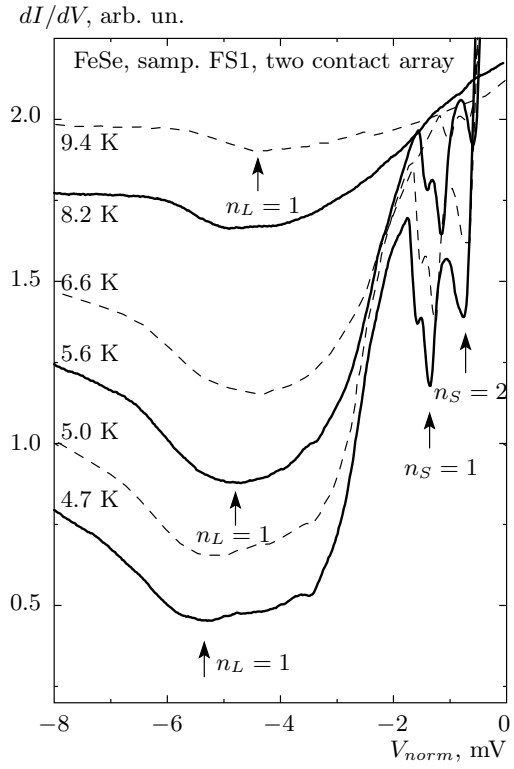


**Fig. 8.** Subharmonic gap structures in $dI/dV$ characteristics of a break junction in FeSe (sample FS1) at different temperatures ($T_C = 12.5$ K). The subharmonic gap structure dips labeled with $n_L$ and $n_S$ are indicated. A close doublet structure of the Andreev singularities for $n_S = 1$ could be result from a four-band nature of the electron spectrum of FeSe [1, 2]

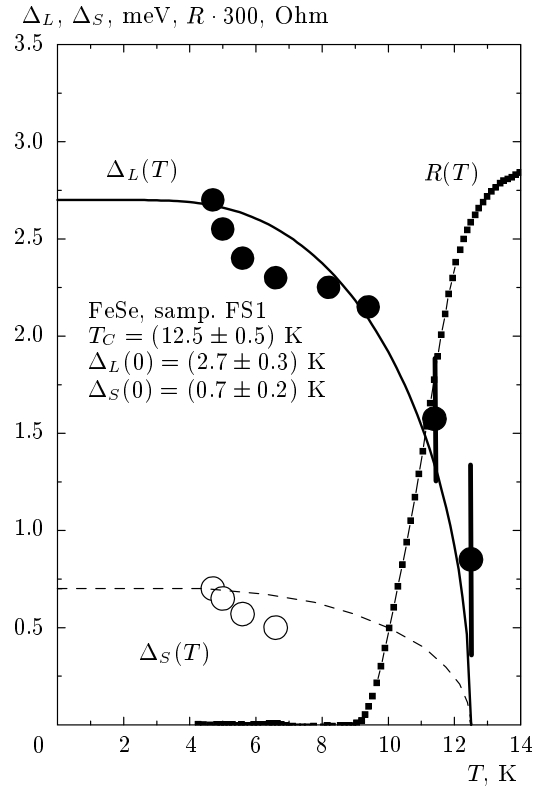


**Fig. 9.** The temperature dependences of the $\Delta_L(T)$ and $\Delta_S(T)$ gaps in FeSe (sample FS1) and the sample resistance $R(T)$ ($T_C = (12.5 \pm 0.5)$ K, $\Delta_L(0) = (2.7 \pm 0.3)$ meV, and $\Delta_S(0) = (0.7 \pm 0.2)$ meV). Solid and dashed lines are the theoretical BCS-type dependences $\Delta(T)$

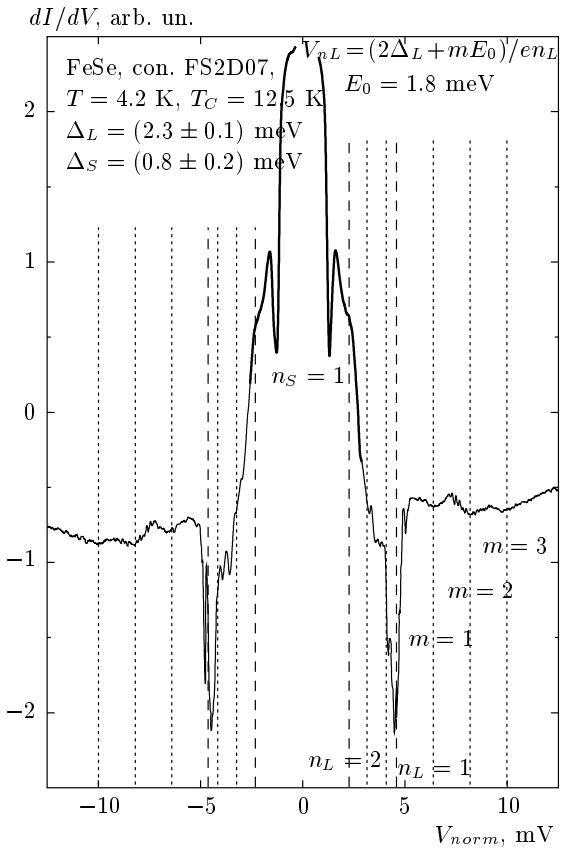


**Fig. 10.** The normalized $dI/dV$ characteristic of the Andreev ScS break junction in a polycrystalline FeSe sample (two-contact array FS2D07, $T_C = 12.5$ K) at $T = 4.2$ K. Two sets of subharmonic gap singularities at the bias voltages $V_{nL} = 2\Delta_L/en_L$ and $V_{nS} = 2\Delta_S/en_S$ are detectable ($\Delta_L = (2.3 \pm 0.2)$ meV and $\Delta_S = (0.8 \pm 0.2)$ meV). An additional fine structure at the bias voltages $V_{nL} = (2\Delta_L + mE_0)/en_L$, marked by dotted lines, is possibly caused by a resonant emission of $m$ Leggett exitons with the energy $E_0 = (1.8 \pm 0.1)$ meV in the process of multiple Andreev reflections ($n_L = 1$)

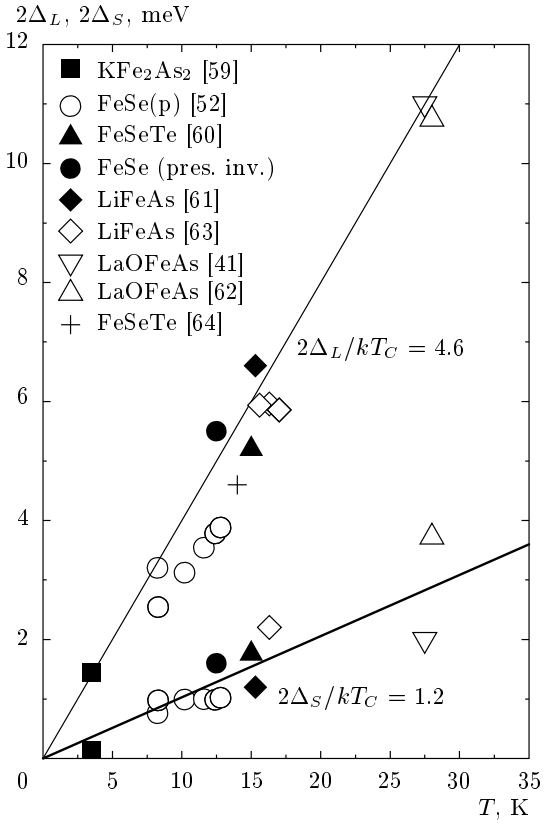


**Fig. 11.** Superconducting gap parameters $2\Delta_L$ and $2\Delta_S$ vs. the critical temperature $T_C$ for iron-based superconductors $KFe_2As_2$ [59], FeSe (under external pressure [52]), $FeTe_{0.5}Se_{0.5}$ [60], $FeTe_{1-x}Se_x$ [64], FeSe (present investigation), LiFeAs [61, 63], $LaFeAsO_{0.9}F_{0.1}$ [41], and $LaFeAsO_{1-x}F_x$ [62]

with the theoretical results in Ref. [53] for an $s$-wave superconductor with a nodeless gap. Theoretical plots of the derivatives of the dynamic conductance $d^2I/dV^2$ vs. the bias voltage [41, 53] display a rather *symmetric* behavior (as in Fig. 4). For a $d$-wave superconductor, a strong asymmetry in the form of the Andreev singularity develops due to the presence of nodes in $\Delta(\varphi)$ [53].

We have observed an additional fine structure in the CVCs of FeSe break junctions at bias voltages $V_{nL} = (2\Delta_L + mE_0)/en_L$ (Fig. 10), which closely resembles the structure caused by a resonant emission of $m$ Leggett plasmons [26] in the process of multiple Andreev reflections in $MgB_2$ contacts [27–29]. If this is the case, the energy of the Leggett plasmon for FeSe $E_0 \approx 1.8 \pm 0.1$ meV is close to $2\Delta_S$ and does not therefore contradict the requirements for the observation of the resonance in a two-band superconductor with nodeless gaps [31].

It was pointed out previously [54–57] that inelastic neutron scattering data can provide a valuable information about the symmetry of the superconducting gap in novel superconductors. Calculations have shown, in particular, that a prominent hump structure unrelated to the resonance mechanism must appear in the dynamic spin susceptibility just above the $2\Delta$ energy in the case of an $s_{++}$-wave state (the fully gapped $s$-wave state without sign reversal) [57]. Recently, the experimental linear dependence of the spin resonance energy $E_{res}$ on $T_C$ with the average slope $4.7kT_C$ was presented for several iron-based superconductors (Fig. 5 in Ref. [58]). Within experimental errors, this depen-

dence is coincident with the plot of the superconducting gap parameter $2\Delta_L$ vs. the critical temperature $T_C$ for FeSe (this investigation) and iron-based superconductors $KFe_2As_2$ [59], FeSe (under external pressure [52]), $FeTe_{0.5}Se_{0.5}$ [60], $FeTe_{1-x}Se_x$ [64], LiFeAs [61, 63], $LaFeAsO_{0.9}F_{0.1}$ [41], and $LaFeAsO_{1-x}F_x$ [62] (Fig. 11). Although the scattering of data is quite significant, two linear dependences emerge with $2\Delta_L/kT_C = 4.6 \pm 0.3$ and $2\Delta_S/kT_C = 1.2 \pm 0.2$ (Fig. 11). The coincidence of $2\Delta_L/kT_C$ (Fig. 11) and $E_{res}/kT_C$ (Fig. 5 in Ref. [58]) supports the version of a fully gapped $s$-wave state without sign reversal [57].

In conclusion, current–voltage characteristics in polycrystalline FeSe samples have been measured using the break-junction technique. The individual ScS Sharvin contacts and stacks of SNS contacts (natural nanosteps-and-terraces structures) show subharmonic gap structures due to multiple Andreev reflections. Two sets of SGSs were detected, indicating the existence of two nodeless superconducting gaps $\Delta_L = (2.75 \pm 0.3)$ meV and $\Delta_S = (0.8 \pm 0.2)$ meV. The layered structure of FeSe allowed observing well-shaped current–voltage characteristics in stacks of Andreev contacts with up to five contacts. An additional fine structure in the CVCs of Andreev ScS nanocontacts is attributed to the existence of a Leggett mode. A linear relation between the superconducting gap $\Delta_L$ and the magnetic resonance energy $E_{magres} \approx 2\Delta_L$ is found to be valid for layered iron pnictides.

This work was supported by the RFBR Grants 08-02-00935, 08-02-90401, and 10-03-91334 and the DFG Grants 436RUS113 and FOR 538/BU887/4. We thank E. G. Maksimov, V. M. Pudalov, and I. A. Yanson for the useful discussions.

## REFERENCES


1. A. L. Ivanovskii, Physics — Uspekhi **51**, 1229 (2008); Yu. A. Izyumov and E. Z. Kurmaev, Physics — Uspekhi **51**, 1261 (2008); M. V. Sadovskii, Physics — Uspekhi **51**, 1201 (2008).
2. D. C. Johnston, Adv. Phys. **59**, 803 (2010).
3. F.-C. Hsu et al., Proc. Nat. Acad. Sci. **105**, 14262 (2008).
4. S. Margadonna et al., Chem. Comm. (Camb.) 5607 (2008).
5. S. Margadonna et al., Phys. Rev. B **80**, 064506 (2009).
6. S. Medvedev et al., Nature Materials **8**, 630 (2009).
7. Y. F. Nie et al., Appl. Phys. Lett. **94**, 242505 (2009).
8. A. J. Williams et al., J. Phys.: Condens. Matter **21**, 305701 (2009).
9. T. M. McQueen et al., Phys. Rev. B **79**, 014522 (2009).
10. M. Bendele et al., Phys. Rev. Lett. **104**, 087003 (2010).
11. Chen Fang et al., EPL **86**, 67005 (2009).
12. M. Johannes, Physics **1**, 28 (2008).
13. A. Subedi, L. Zhang, D. J. Singh, and M. H. Du, Phys. Rev. B **78**, 134514 (2008).
14. V. A. Moskalenko, Phys. Met. Metall. **4**, 503 (1959).
15. H. Suhl et al., Phys. Rev. Lett. **12**, 552 (1959).
16. V. Z. Kresin and S. A. Wolf, Phys. Rev. B **46**, 6458 (1992).
17. S. D. Adrian et al., Phys. Rev. B **56**, 7878 (1997).
18. N. Klein et al., Phys. Rev. Lett. **71**, 3355 (1993).
19. B. A. Aminov et al., J. Supercond. **7**, 361 (1994).
20. Ya. G. Ponomarev, Physica C **243**, 167 (1995).
21. J. Nagamatsu et al., Nature (London) **410**, 63 (2001).
22. Y. Kamihara et al. J. Amer. Chem. Soc. **130**, 3296 (2008).
23. X. X. Xi, Rep. Progr. Phys. **71**, 116501 (2008).
24. R. Khasanov et al., Phys. Rev. B **78**, 220510 (2008).
25. J. K. Dong et al., Phys. Rev. B **80**, 024518 (2009).
26. A. J. Leggett, Progr. Theor. Phys. **36**, 901 (1966).
27. Ya. G. Ponomarev et al., Sol. State Comm. **129**, 85 (2004); Ya. G. Ponomarev et al., arXiv:cond-mat/ /0303640.
28. Ya. G. Ponomarev et al., JETP Lett. **85**, 46 (2007).
29. A. E. Karakozov, E. G. Maksimov et al., JETP Lett. **91**, 24 (2010).
30. G. Blumberg et al., Phys. Rev. Lett. **99**, 227002 (2007).
31. F. J. Burnell et al., Phys. Rev. B **82**, 144506 (2010).
32. R. Kleiner and P. Müller, Physica C **293**, 156 (1997).
33. H. Nakamura et al., J. Phys. Soc. Jpn. **78**, 123712 (2009).
34. T. Koyama et al., Physica C **470**, 1481 (2010).
35. Yu. Koval et al., 2009 APS March Meeting, #P35.003.
36. Yi. Yin et al., Physica C **469**, 535 (2009).

**37**. D. Daghero et al., Supercond. Sci. Technol. **23**, 043001 (2010).

**38**. T. Y. Chen et al., Physica C **469**, 521 (2009).

**39**. R. S. Gonnelli et al., Physica C **469**, 512 (2009).

**40**. P. Samuely et al., Physica C **469**, 507 (2009).

**41**. Ya. G. Ponomarev et al., Phys. Rev. B **79**, 224517 (2009).

**42**. Yu. V. Sharvin, Zh. Eksp. Teor. Fiz. **48**, 984 (1965).

**43**. T. Kamimura, J. Phys. Soc. Jpn. **43**, 1594 (1977); H. Ikeda, M. Shirai, N. Suzuki, and K. Motizuki, J. Magn. Magn. Mater **140–144**, 159 (1995).

**44**. C. J. Muller et al., Physica C **191**, 485 (1992).

**45**. R. Kümmel et al., Phys. Rev. B **42**, 3992 (1990).

**46**. G. E. Blonder et al., Phys. Rev. B **25**, 4515 (1982); M. Octavio et al., Phys. Rev. B **27**, 6739 (1983); K. Flensberg et al., Phys. Rev. B **38**, 8707 (1988).

**47**. A. Poenicke et al., Phys. Rev. B **65**, 220510 (2002).

**48**. Ya. G. Ponomarev et al., Inst. Phys. Conf. Ser. **167**, 241 (2000); Ya. G. Ponomarev et al., Phys. Stat. Sol. C **6**, 2072 (2009).

**49**. H. Schmidt, M. A. Lorenz, G. Muller et al., in: *Abstracts, 6th Intern. Conf. M2SHTSC-VI*, Feb. 20–25 (2000), Houston, Texas, 2C2.6, p. 170.

**50**. T. Katase et al., arXiv:0907.0666.

**51**. M. Hurd et al., Phys. Rev. B **54**, 6557 (1996).

**52**. R. Khasanov et al., Phys. Rev. Lett. **104**, 087004 (2010).

**53**. T. P. Devereaux and P. Fulde, Phys. Rev. B **47**, 14638 (1993).

**54**. M. Eschrig, Adv. Phys. **55**, 47 (2006).

**55**. T. A. Maier and D. J. Scalapino, Phys. Rev. B **78**, 020514 (2008).

**56**. G. Yu et al., Nature Phys. **5**, 873 (2009).

**57**. S. Onari et al., Phys. Rev. B **81**, 060504 (2010).

**58**. Shin-ichi Shamoto et al., Phys. Rev. B **82**, 172508 (2010).

**59**. H. Fukazawa, J. Phys. Soc. Jpn. **78**, 083712 (2009).

**60**. P. K. Biswas et al., Phys. Rev. B **81**, 092510 (2010).

**61**. K. Sasmal et al., Phys. Rev. B **81**, 144512 (2010).

**62**. M. Yashima et al., J. Phys. Soc. Jpn. **78**, 103702 (2009).

**63**. Y. Imai et al., J. Phys. Soc. Jpn. **80**, 013704 (2011).

**64**. T. Kato et al., Phys. Rev. B **80**, 180507R (2009).